DOI 10.5162/iCCC2026/P24

Effects of Surface Functionalization on Convective Heat Transfer with Relevance to Heat Exchanger Engineering

Sai Ravi Gupta Polasanapalli[1,2], Marten Klein[1,2], and Heiko Schmidt[1,2]

[1]Chair of Numerical Fluid and Gas Dynamics, BTU Cottbus-Senftenberg, 03046 Cottbus, Germany
[2]Scientific Computing Lab, Energie-Innovationszentrum (EIZ), BTU, Cottbus-Senftenberg, 03046 Cottbus, Germany
E-Mail-Address: SaiRaviGupta.Polasanapalli@b-tu.de

Abstract

This study investigates how wall surface properties affect fluid motion and heat transfer in an idealized natural convection setup. Natural convection in a cubic box with a heated bottom wall and a cooled top wall is used as a simplified setup to analyze heating and cooling efficiency for regular (no-slip), free-slip, and coated (finite-slip) walls. Using a three-dimensional lattice Boltzmann method (LBM) solver in direct numerical simulation (DNS) mode, simulations are performed for three Prandtl numbers Pr = 0.786, 4.38, and 10, and two Rayleigh numbers Ra = 2×10^6, and 10^7. The aim is to understand how surface conditions influence flow patterns, thermal mixing, and heat transfer efficiency. Results show that free-slip conditions significantly enhance heat transfer, yielding higher Nusselt numbers due to thinner thermal boundary layers and stronger convective currents. The results demonstrate that surface boundary conditions play a role in modulating flow dynamics and heat transfer in RB convection.

1 Introduction

Energy efficiency and effective thermal management are key challenges in modern energy systems, ranging from conventional power plants to renewable energy technologies. Improving heat transfer performance directly enhances system efficiency, reliability, and sustainability. One promising strategy to achieve this involves modifying the properties of solid surfaces in contact with fluids. In particular, hydrophobic and super-hydrophobic coatings have attracted attention because they can change how fluids move close to a wall, potentially reducing flow resistance [1] and improving heat transfer performance [2, 3]. Such surface effects are particularly important because even thin surface layers or coatings can significantly influence thermal performance. In practical heat exchangers, for example, the formation of thin rough material layers on internal surfaces can lead to rapid efficiency losses of about 10–15%, highlighting the strong sensitivity of heat transfer to surface conditions.

Understanding how wall conditions affect turbulent heat transfer is therefore crucial for the design and operation of energy-efficient thermal systems. In this context, Rayleigh–Bénard (RB) convection serves as a canonical model for buoyancy-driven heat transfer and is relevant to applications such as heat exchangers, solar thermal collectors, nuclear reactor cooling, and geothermal energy systems [4].

In this study, the natural convection in a box is studied as an idealized setup that enables quantitative analysis of heating/cooling efficiency under the influence of functionalized (coated) walls. Specifically, we examine no-slip, free-slip, and finite-slip boundary conditions with slip lengths in the range slip-lengths l_s = 0.00005m to 0.0005m. Three-dimensional numerical simulations are performed using a lattice Boltzmann method (LBM) solver, which is well-suited for efficient upscaling to high Rayleigh number regimes with strong thermal forcing. The LBM solver operates in direct numerical simulation (DNS) mode, ensuring full-scale resolution of the flow dynamics. The primary objective is to examine the effects of no-slip, free-slip, and finite-slip wall conditions on flow and heat transfer characteristics for fluids and chemical solvents with different Prandtl numbers. The results provide insights into optimizing thermal performance through surface control.

2 Simulation Setup

Figure 1(a) depicts the schematic representation of the RB cell under investigation. The computational domain is defined as H × H × H in the x, y, and z directions, where H represents the height of the cubic cavity, serving as the characteristic length scale. The bottom wall is at a higher temperature (T_h), while the top wall is at a lower temperature (T_c). Temperature boundary conditions on the vertical walls are considered as adiabatic walls. The flow and heat transfer in the RB system are governed by the Rayleigh and Prandtl numbers. The Rayleigh number represents the strength of buoyancy-driven convection relative to viscous and diffusive effects, while the Prandtl number describes the relative rates of momentum and thermal diffusion in the fluid. Together, these parameters determine the convection regime and heat transfer characteristics. In our study, we explore three distinct velocity boundary conditions, namely, no-slip, free-slip, and finite-slip, applied to all walls. The finite-slip condition is a commonly used mathematical framework for modelling hydrophobic and super-hydrophobic wall behaviour. It is given by Navier-slip is shown in **Figure 1(b)**. The Navier slip length (l_s), defined as the distance from the wall to the point where the extrapolated wall-parallel velocity component vanishes, is a standard choice

DOI 10.5162/iCCC2026/P24

[5]. A slip length of zero corresponds to a no-slip wall, while an infinite slip length represents a free-slip wall. Typical slip lengths range from 100 nm for hydrophobic surfaces to 100 μm for super-hydrophobic surfaces.

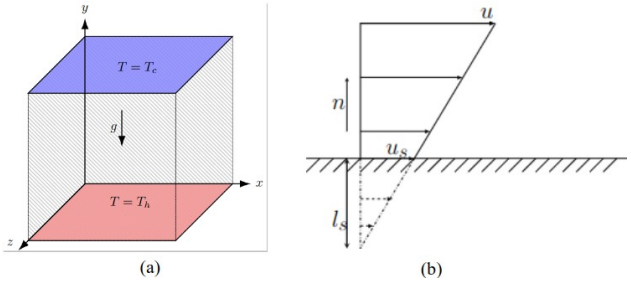

Figure 1 Schematic diagrams. (a) Slip velocity representation (b) RB convection in a cubic cavity.

Furthermore, a non-uniform grid is employed throughout the domain, with a finer grid resolution being used near the walls. Initial perturbations [6] are imposed to facilitate the transition of the flow from a laminar to a turbulent state. In the current investigation, an in-house off-lattice Boltzmann method solver [7, 8] is employed in the DNS mode for conducting simulations. The present implementation relies on a finite-difference-based framework for non-isothermal flows in the linear Oberbeck–Boussinesq regime. The LBM collision term is treated implicitly to improve the numerical stability of the scheme. Accurate characteristic-based treatment (of streaming) is obtained by a Lax–Wendroff scheme for time integration of the LBM equations. An explicit second-order central-difference scheme is used to discretize the advection terms. A sixth-order compact spatial filter is employed to remove oscillations caused by non-dispersive central difference schemes.

3 Results and Discussions

The simulations reveal significant differences in flow organization and heat transfer depending on the boundary conditions, as shown in **Figure 2** and **3**. For free-slip walls, a single large-scale vortex dominates the flow, enhancing coherent fluid motion and reducing flow reversal. In contrast, no-slip and finite-slip conditions produce smaller, chaotic vortices. This behavior arises from the fundamental distinction between the two conditions: free-slip walls permit tangential fluid motion along the boundary, whereas no-slip surfaces enforce zero fluid velocity at the boundary with a sharp velocity gradient. This high non-linearity in the no-slip case is the primary driver behind the formation of multiple eddy recirculation zones. Consequently, larger velocity fields are observed in the free-slip cases compared to the no-slip surface cases, resulting in a thinner thermal boundary layer thickness that significantly impacts the heat transfer rate. The free-slip condition on vertical walls significantly influences vortex structures, while free-slip on horizontal walls enhances velocity magnitudes and heat transfer.

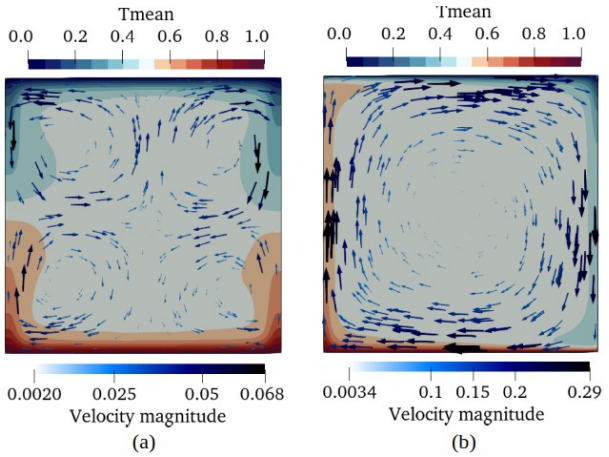

Figure 2 Mean velocity vectors and temperature distribution on the mid spanwise plane for temporal and spanwise averaged quantities. (a) No-slip (b) Free-slip.

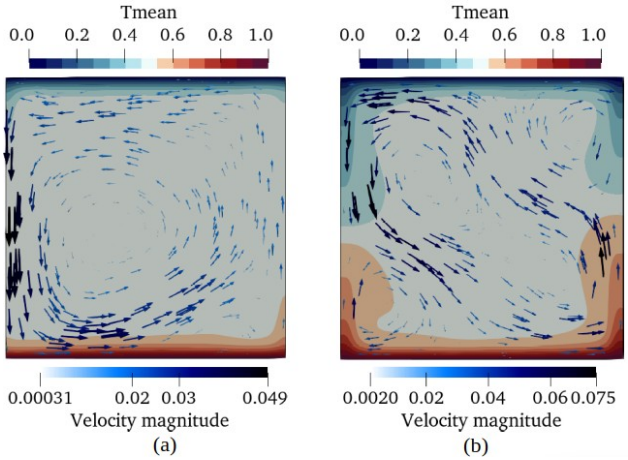

Figure 3 Mean velocity vectors and temperature distribution on the mid spanwise plane for temporal and spanwise averaged quantities. (a) Free-slip-Side (b) Slip-8.

Figures 4 and **5** show the horizontal (x-z-plane) averages of statistical quantities along the vertical axis for different boundary conditions at Ra = 2×10^6 and Pr = 4.38. The non-dimensionalized mean temperature profile along the cavity height is presented in **Figure 4(a)**. Under free-slip boundary conditions, the flow velocity is larger, leading to a thinner thermal boundary layer compared to the no-slip case, where a steeper gradient near the walls and uniformity in the central region is prominent. **Figure 4(b)** illustrates the non-dimensionalized vertical velocity component profile, where all cases, except FS and FS-side, exhibit a two-peak structure with a central dip, consistent with the (2, 2) vortex mode pattern in the flow as described above. By contrast, the free-slip cases FS and FS-side exhibits a parabolic profile variation, so that larger velocity values are present at the cavity center. Overall, the free-slip cases FS, FS-hori, and FS-side show larger velocity magnitudes than the no-slip case NS. Although the finite-slip cases deviate slightly from the no-slip case, they exhibit a similar overall profile. Finite-slip cases, positioned between no-slip and free-slip conditions, fall closer to no-slip behavior due to the use of small slip lengths.

DOI 10.5162/iCCC2026/P24

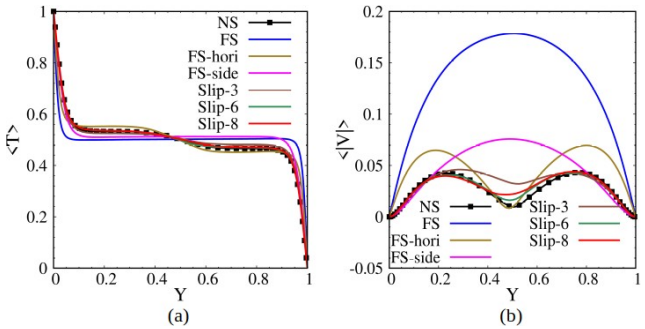

Figure 4 Normalized vertical profiles of horizontally averaged mean quantities. (a) Mean temperature (b) Mean vertical velocity magnitude.

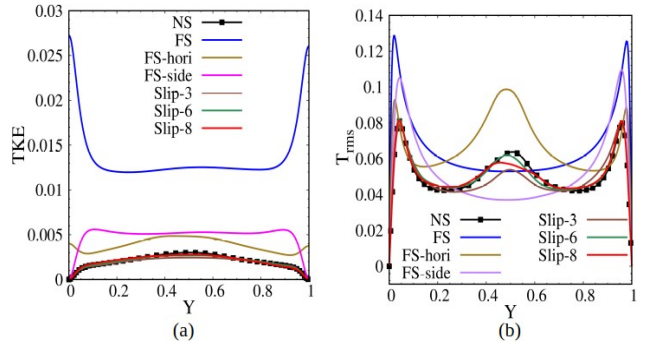

Figure 5 Normalized vertical profiles of horizontally averaged fluctuation quantities. (a) Turbulent kinetic energy (b) Temperature RMS fluctuations.

Figure 5(a) shows the distribution of turbulence intensity (turbulent kinetic energy) along the cavity height. The zero shear stress at the boundary in free-slip cases can lead to more intense turbulence, as the fluid near the walls experiences less resistance and can move more freely. Consequently, the turbulent kinetic energy (TKE) is generally higher for the FS case than the no-slip case. Although the slip cases show minor deviations from each other due to variations in slip length and anisotropy, their profiles largely resemble that of the no-slip case. Finally, **Figure 5(b)** illustrates the intensity of temperature fluctuations, quantified using the root mean square (RMS). The temperature RMS shows two peaks near the walls and a smaller peak at the center. However, in the case with a free-slip condition on the vertical sidewalls, the central peak disappears, and lower values are observed in the central region. The temperature RMS values are larger near the walls in free-slip due to more intense thermal mixing and less temperature fluctuations in the central region because the fluid near the boundaries is not as restricted by the no-slip condition, leading to a more uniform temperature distribution in the core. The temperature RMS variation in finite-slip cases is similar to that of the no-slip case.

The overall heat transfer rate for different wall conditions is quantified using the Nusselt number and reported in **Table 1**. The effects of different slip lengths and wall orientations, such as horizontal and vertical, are also reported at Ra = 2×10^6 and Pr = 4.38. Case names NS, FS, FS-side, FS-hori, and Slip 1-8 represent the following conditions: no-slip, free-slip on all walls, free-slip on vertical side walls, free-slip on horizontal walls, and finite-slip cases, respectively. The heat transfer rates are highest for free-slip conditions, with Nu increasing by up to 100% compared to no-slip cases. Because, in free-slip cases, the fluid experiences no frictional resistance at the walls, allowing for higher flow velocities near those boundaries. This results in a thinner thermal boundary layer, which significantly enhances the heat transfer rate. Finite-slip conditions with changing slip lengths also, however, show only marginal improvements over no-slip. The effect of surface condition on heat transfer rate for different fluids is presented in **Table 2**. The free-slip condition consistently yields higher Nusselt numbers compared to no-slip and finite-slip conditions across all Prandtl numbers investigated. Notably, the enhancement in heat transfer is most pronounced for Pr = 10, where the Nusselt number increases by 170% compared to the no-slip case. This is attributed to the combined effects of reduced viscous damping and enhanced thermal gradients at higher Prandtl numbers. Finite-slip boundary conditions result in heat transMean velocity vectors and temperature distri- bution on the mid spanwise plane for temporal and span- wise averaged quantities.fer rates that are nearly identical to those observed for no-slip conditions at all Prandtl numbers. This suggests that the finite-slip length considered here (l_s = 0.0005) is insufficient to significantly alter the flow dynamics or heat transfer characteristics compared to the no-slip condition. At the higher Rayleigh number Ra = 10^7 and Pr = 4.38, the heat transfer rates are significantly higher due to the increased buoyancy-driven turbulence. These results indicate that the finite-slip boundary conditions result in only minor changes in heat transfer at high Rayleigh numbers. A small increment in the Nusselt number is observed for the finite-slip case, l_s = 0.0001. Even at higher turbulent Rayleigh numbers, the effect of partial slip on heat transfer remains limited for the slip lengths considered in this study.

Case	Nu
NS	9.97
FS	19.99
FS-hori	15.97
FS-side	11.14
Slip-1	10.01
Slip-2	10.09
Slip-3	10.43
Slip-4	9.90
Slip-5	10.22
Slip-6	10.10
Slip-7	10.45
Slip-8	9.68

Table 1 Heat transfer in terms of Nusselt number Nu for various surface conditions at Ra = 2×10^6 and Pr = 4.38.

DOI 10.5162/iCCC2026/P24

Ra	Pr	Walls	Nu
2×10^6	0.786	No-slip	10.27
		Free-slip-all	21.43
		Slip l_s= 0.0005	10.30
	4.38	No-slip	9.97
		Free-slip-all	19.99
		Slip l_s= 0.0005	9.9
	10	No-slip	9.81
		Free-slip-all	26.55
		Slip l_s= 0.0005	9.75
10^7	4.38	No-slip	16.76
		Slip l_s= 0.0001	17.27
		Slip l_s= 0.0005	16.74

Table 2 Overall Nusselt number for various surface conditions and different fluids in terms of Pr and Ra.

Figure 6 shows how the flow patterns change when the wall condition is switched from a regular wall (no-slip) to a functionalized wall (free-slip). The comparison is made using the Lumley triangle analysis [9]. The anisotropy line is drawn along the central vertical axis. The influence of the walls on the turbulent states remains distinctly evident. In the no-slip case, a multitude of turbulent states is observed when moving from the bottom wall to the top wall, whereas a dominant single-component axisymmetric turbulent state is presented in the free-slip case. The comparison shows how surface boundary conditions fundamentally alter the nature of turbulence anisotropy, with free-slip walls promoting a simplified turbulent state relative to the more complex and spatially varying turbulence observed under no-slip conditions.

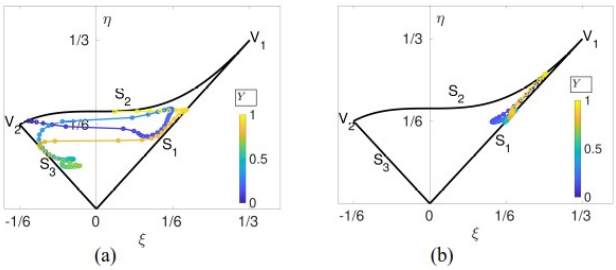

Figure 6 Lumley flow anisotropy analysis across the cavity height y (color) for the two velocity boundary conditions investigated. (a) No-slip (b) Free-slip.

4 Conclusions

In this study, we examined how different wall surface properties affect fluid motion and heat transfer in a heated and cooled system. We compared regular walls, where the fluid sticks to the surface, with coated walls, where the fluid can slide along the surface more easily. Using detailed computer simulations, we found clear differences in how the fluid moves and how heat is transported. Free-slip conditions resulted in an unsteady large-scale circulation pattern and enhanced heat transfer due to higher mean velocities and steeper temperature gradients near walls. In contrast, no-slip conditions exhibited diverse turbulent modes and flow reversals. The results highlight that wall boundary-slip can be a viable passive strategy to control thermal convection performance.

5 Acknowledgement

This research is supported by the German Federal Government, the Federal Ministry of Research, Technology and Space, and the State of Brandenburg within the framework of the joint project EIZ: Energy Innovation Center (project numbers 85056897 and 03SF0693A) with funds from the Structural Development Act (Strukturstärkungsgesetz) for coal-mining regions. Provision of computing resources by the National High Performance Computing Alliance (NHR-NORD@Göttingen) under the project number bbi00022 is also gratefully acknowledged.

6 References

[1] Choi, C.-H.; Kim, C.-J.: Physical Review Letters 96 (2006) H. 6, S. 066001.

[2] Mayeed, M. S.; Patnaik, S. S.; Mitchell, R.: In Proceedings of the ASME 2016 International Mechanical Engineering Congress and Exposition (IMECE2016). USA: ASME, 2016.

[3] Wu, C. H.; Huang, Y. S.; Kuo, L. S.; Chen, P. H.: International Journal of Heat and Mass Transfer 63 (2013) S. 249–254.

[4] Chillà, F.; Schumacher, J.: European Physical Journal E 35 (2012) H. 6, S. 58.

[5] Rothstein, J. P.: Annual Review of Fluid Mechanics 42 (2010) H. 1, S. 89–109.

[6] Schoppa, W.; Hussain, F.: Fluid Dynamics Research 26 (2000) H. 2, S. 119.

[7] Polasanapalli, S. R. G.; Anupindi, K.: Physics of Fluids 34 (2022) H. 3, S. 035125.

[8] Polasanapalli, S. R. G.; Anupindi, K.: International Journal of Heat and Mass Transfer 225 (2024) S. 125395.

[9] Lumley, J. L.: Advances in Applied Mechanics 18 (1979) S. 123–176.